

Confined Plasmons in Metallic Nanocavities

S. Coyle,¹ M. C. Netti,¹ J. J. Baumberg,¹ M. A. Ghanem,² P. R. Birkin,² P. N. Bartlett,² and D. M. Whittaker¹

¹*Department of Physics and Astronomy, University of Southampton, Southampton SO17 1BJ, United Kingdom*

²*Department of Chemistry, University of Southampton, Southampton SO17 1BJ, United Kingdom*

(Received 25 May 2001; published 2 October 2001)

We investigate the properties of gold surfaces patterned using a nanoscale “lost wax” technique by electrochemical deposition through a self-assembled latex template. Near-spherical nanocavities within the resulting porous films support localized surface plasmons which couple strongly to incident light, appearing as sharp spectral features in reflectivity measurements. The energy of the resonances is easily tunable from ultraviolet to near infrared by controlling the diameter and height of the nanocavities. The energies of these features agree well with the Mie resonances of a perfect spherical void.

DOI: 10.1103/PhysRevLett.87.176801

PACS numbers: 73.20.Mf, 42.70.Qs, 78.20.Bh, 81.07.-b

Metals are highly reflective because their electrons cannot absorb energy at optical frequencies which are below the plasma frequency of their charge oscillations, which lie in the UV. Metal-dielectric interfaces support a 2D blend of photon and plasmon known as surface plasmon polaritons with frequencies in the visible part of the spectrum. On a smooth surface, these cannot interact with incident light thus preserving the high reflectivity. In contrast, metal surfaces which are roughened on the scale of the optical wavelength can couple to light and become colored due to selective surface-plasmon absorption, an effect known since the papers of Wood on metallic gratings [1]. This effect is directly exploited for surface-enhanced Raman scattering in sensing applications. Recently there has been much interest in metallic films drilled with regular patterns of submicron holes which show enhanced transmission at specific wavelengths and evidence photonic band structure [2,3]. Another approach to plasmon engineering has been through growth of subwavelength metal particles, in which the surface plasmons break up into discrete modes [4–6]. However, it is nontrivial to size select and support separately such metal spheres in a solid matrix.

Here we demonstrate a new approach to confining plasmons using an electrochemically patterned surface formed by a nanoscale “lost wax” casting. The resulting gold film consists of near-spherical nanocavities surrounded by metal, which completely laterally confine the surface plasmons. In contrast to periodic patterning of dielectrics [7], metals [2,8], or metallodielectrics [9] which can produce photonic crystals, here the negative nanocavity curvature localizes the electromagnetic fields into small volumes. The photonic properties are thus independent of the geometrical arrangement of nanocavities, simplifying fabrication. We show that plasmons on these negative curvature surfaces can couple very effectively to incident light, unlike metallic spheres, and so show up in reflectivity spectra as strong omnidirectional features which can be widely tuned through the growth morphology. These microstructures are remarkably simple to fabricate as mechanically robust films and demonstrate the principle of plasmon en-

gineering in reduced dimensionalities for photonic and sensing applications.

The photonic metal films were prepared by electrochemical reduction of metal complex ions dissolved in aqueous solution within the interstitial spaces between polystyrene latex spheres self-assembled onto a gold-coated surface [10]. These sphere arrays were crystallized from colloidal solution by controlled evaporation over several days. The latex sphere templates were subsequently removed by dissolving in toluene to leave the structured metal film, as in lost-wax casting (Fig. 1). This simple and versatile technique can be used for a wide variety of metals (e.g., Au, Pt, Co) and polymers and can be calibrated so that control of the total charge passed allows deposition to a precise thickness, t . The resulting mesh reflects the order of the self-assembled template, allowing convenient control of the pore diameters (here using spheres of diameter 0.2, 0.5, 0.7, and 1.0 μm) and local crystalline order.

Preparing a sample which is graded in thickness (by allowing the plating solution to slowly drain from the electrochemical cell) allows the electrochemical growth to be followed using scanning electron micrographs of the top surface (Fig. 1). Initially the gold forms a circular dish

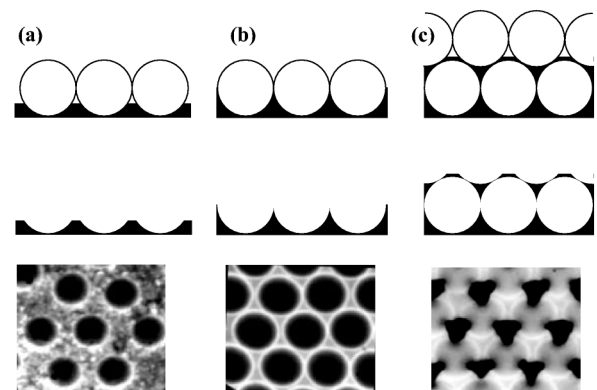


FIG. 1. Schematic cross section of metal film growth and corresponding scanning electron micrographs (below) of the gold nanocavities fabricated with $a = 350$ nm latex spheres, of thickness t of (a) $a/2$, (b) a , and (c) $2.1a$.

(a), growing to a hemispherical cavity (b), but the diffusion-reaction limited nature of the aggregation is geometrically hindered by the next layer of latex spheres, which prevents the cavity from completely closing. The metal grows up around the polystyrene spheres in the upper layer from three columns of metal extending up through the three gaps between the spheres in the layer below [10]. Thus a threefold symmetric pattern of interlinked holes forms (c) connecting the next hemispherical cavities to those below. This mesostructure is repeated in subsequent layers above.

The local optical reflectivity of the macroporous metal films is measured using a white-light laser focused to a $10\ \mu\text{m}$ diameter spot [11]. Typical reflection spectra at 45° incidence, for latex spheres of radius $a = 350\ \text{nm}$, are shown in Figs. 2(a) and 2(b) for different Au thicknesses. These display strong dips that are not generated by patterned Pt [Fig. 2(c)] or Au unpatterned films. Although the short-range order of the latex sphere array can be good (Fig. 1), the crystal grains here are typically a few μm across, resulting in an amorphous microstructure which suppresses diffraction. This is confirmed by the insensitivity of the spectra to the in-plane (azimuthal) orientation of the metallic nanostructure [Fig. 2(d)]. As the angle of incidence is changed, the resonant dips vary in strength and TE/TM ratio but show minimal energy shifts. When we examine more ordered crystallites a complicated structure is seen which becomes dependent on the nanostructure orientation, to be discussed elsewhere. Extinction ratios in excess of 20 dB are found and up to three resonances are seen simultaneously. In particular, a range

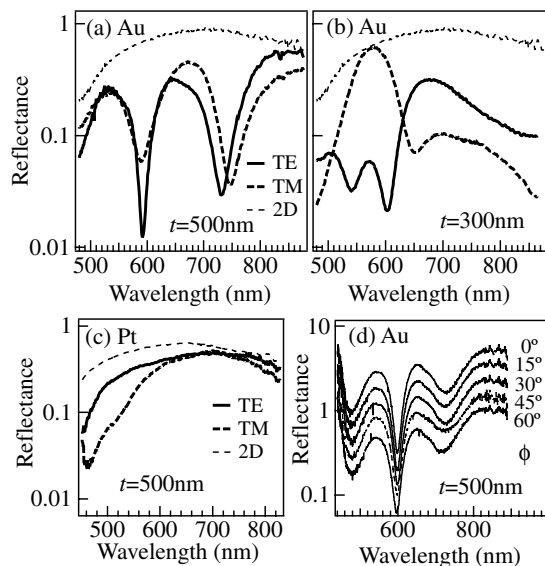


FIG. 2. Reflectivity spectra on a graded sample ($a = 350\ \text{nm}$) at different locations for both TE and TM polarized incident light at 45° and Au thickness of (a) $500\ \text{nm}$ and (b) $300\ \text{nm}$. The dotted curve is an unpatterned film electrodeposited under the same conditions. (c) Similarly patterned and unpatterned Pt sample of thickness $500\ \text{nm}$. (d) Au sample reflectivity (a) at increasing azimuthal angles, ϕ .

of film thicknesses is found for which the TE and TM resonances are sharp ($<20\ \text{nm}$ half-widths) and nearly coincident [Fig. 2(a)]. By correlating the microstructure with the resonant energies we can confirm these modes arise from zero-dimensional plasmons trapped inside the Au cups.

Electron microscopy allows direct confirmation of the film thickness, through measurement of the size and shape of the pore openings at the sample surface. The extracted energies of the modes are shown in Figs. 3(a) and 3(b) for TE, TM incident polarizations. When the cups in the growing gold film are small, the frequencies change only slowly. However, near the half-height thickness ($t \sim a$) the modes rapidly shift to longer wavelengths (region I). This is exactly the opposite behavior to that expected for interference on a length-scale set by the rim circumference of the nanocavity—the diameter changes rapidly for the thinnest layers and barely changes near the half-height thickness, suggesting that “rim” plasmons are not supported. Subsequently the mode frequencies change little until close to the full height thickness ($t \sim 2a$, region II). Again this insensitivity suggests that the cavity aperture does not directly control the resonance. Only at the interface between two layers of latex spheres does the optical extinction

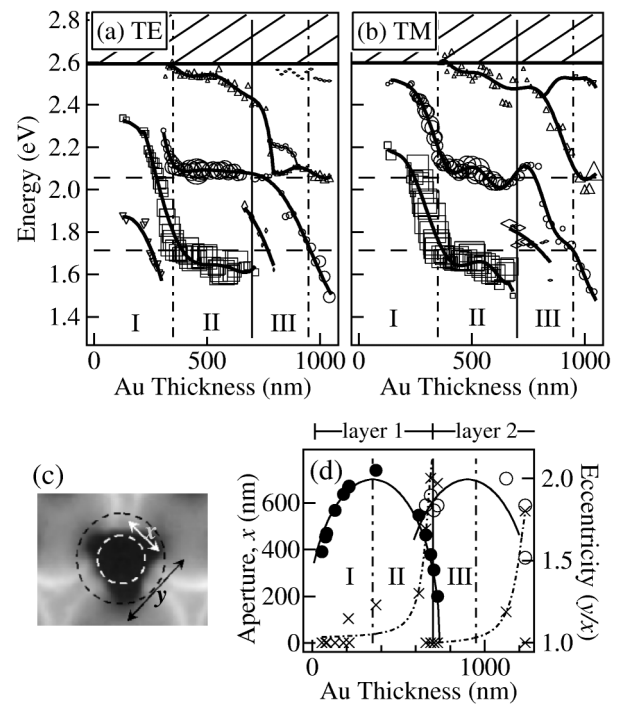


FIG. 3. (a,b) Extracted mode energies for TE, TM polarizations at an angle of incidence of 45° . The symbol size indicates the mode sharpness (depth/linewidth). The vertical lines mark the heights of $\frac{1}{2}$, 1 , $\frac{3}{2}$ spheres ($a = 350\ \text{nm}$), and above $2.6\ \text{eV}$ planar surface plasmon absorption occurs. Horizontal lines are solutions of the spherical void model for $\ell = 2, 3$. (c) Nanocavity aperture parametrized by circumscribed and inscribed diameters. (d) Aperture characteristics for different Au thickness defined by the minimum aperture diameter for the lowest (\bullet) and second (\circ) layers and their eccentricity (\times). The lines are guides to the eye.

become strong, producing “black” gold. At larger thicknesses the nanostructures repeat, and similar modes are seen once the highly eccentric transition region is passed (region III). The modes emerge from the short wavelength limiting value of the 2D plasmon frequency for gold and are not observed on similar Pt and Co mesoporous films. Plasmons in Pt and Co are at higher energy and strongly damped by coupling to interband transitions. Thus we attribute the modes here to fully localized surface plasmons inside cups of Au and understand the independence of the mode frequencies in the enclosed nanocavities in region II from the ability of plasmons to travel in the interior around the equatorial circle.

Full solutions of Maxwells’ equations through photonically patterned metals are complicated by the strength of the coupling between propagating plasmons with different wave vectors. This is the opposite regime to weak coupling found in dielectric photonic crystals [7] in which a perturbative approach is tractable. Previous work on photonic metals has focused on the use of regular arrays of corrugations or holes of a lateral size much less than optical wavelengths. These produce complex and highly directional performance due to their periodicity [2,3,8,12,13] but suggest that plasmons can be trapped, which we are able to confirm here. The solution for plasmons on metal spheres is well known and analytic for radii small enough to allow a nonretarded approximation [14] (i.e., $a \ll \lambda$). Here we extend the solution to spherical metal voids on the scale of the plasmon wavelength ($a \sim \lambda$) which provides an intuitive explanation for our observations.

We consider a simple model of the plasmon-polariton modes supported by a spherical void, of radius a , in an infinite metallic medium. Following Ref. [15] we satisfy continuity of the tangential field components, giving TM modes in the spherical geometry (with electric field parallel to the sphere surface [16]) which satisfy

$$\varepsilon_i H_\ell(k_m a) [k_i a J_\ell(k_i a)]' = \varepsilon_m J_\ell(k_i a) [k_m a H_\ell(k_m a)]', \quad (1)$$

where J_ℓ and H_ℓ are spherical Bessel and Hankel functions, and the prime denotes differentiation with respect to the argument (ka). ε_i and ε_m are the dielectric constants inside and outside the sphere, with $k_i = \sqrt{\varepsilon_i} \omega/c$ and $k_m = \sqrt{\varepsilon_m} \omega/c$ the corresponding wave numbers. We take $\varepsilon_i = 1$ and assume that the external medium is an “ideal” metal with $\varepsilon_m(\omega) = 1 - \omega_p^2/\omega^2$, where ω_p is the 3D plasmon frequency. If frequencies are expressed in units of ω_p , the solutions to Eq. (1) then depend only on the angular momentum quantum number, ℓ , and the normalized sphere radius $R = a\omega_p/c$. Symmetry requires that they degenerate with respect to the azimuthal quantum number, m .

Figure 4(a) shows the calculated plasmon-polariton dispersions for various values of the normalized radius, R , comparable to those in the experiments. The dispersions

are plotted as a function of ℓ/R , which has the dimensions of a wave number. In the limit of large radii ($R \gg 1$), where the surface is effectively flat on the scale of the plasmon wavelength, the dispersion plotted in this way lies on top of that of a 2D planar surface-plasmon polariton plotted vs k (solid line in Fig. 4). For finite R , the negative curvature of the inner void surface causes the energies to shift *above* the planar values. This contrasts to the positive curvature of the exterior surface of a metallic sphere, where the shift is in the opposite direction.

The dashed line in Fig. 4 indicates the light line plotted vs k on the same scale: the photon dispersion in air for propagation along a planar surface. Its significance in the 2D geometry is that it separates states which can decay radiatively, lying above the light line, from those below which are confined to the surface, with only an evanescent field outside. In the real spherical geometry, this distinction is no longer absolute, as any angular momentum state can couple to all external plane waves. However, it is reasonable to expect that for large radii, $R > 1$, there should be a qualitative difference, with states above the

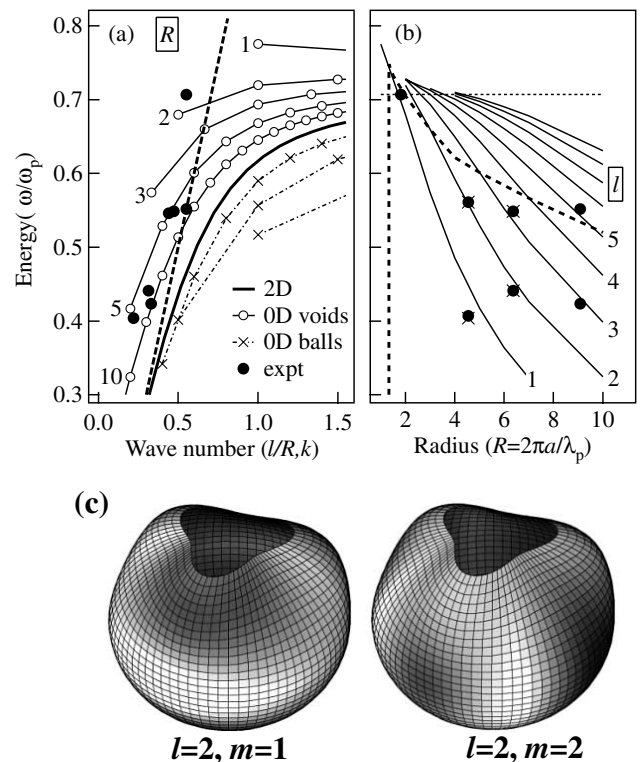


FIG. 4. (a) Localized plasmon energies (normalized to the 3D plasmon energy) for spherical gold voids (\bullet) and spheres (\times) of different radii and angular momentum. Also plotted vs k is the 2D surface-plasmon polariton dispersion (thick line) and the photon dispersion in air (dashed line). (b) Calculated plasmon-polariton energy levels labeled by angular momentum (ℓ) for different radius (a) spherical voids compared to experiment (at thickness $t = 0.75a$). The region below the dashed line is accessible to incoming photons. (c) Calculated radial electric fields on the surface of the microcavity for $(\ell, m) = (2, 1)$ and $(2, 2)$ (dark section corresponds to strongest field).

light line coupling strongly to external photons, and those below only weakly. Of course, in our simplified model with an infinite external medium, no external coupling occurs, but these considerations will nevertheless apply for the coupling in real structures. The angular momentum ℓ of the observed states is assigned using Fig. 4(b), allowing them to be plotted on the dispersion relation [Fig. 4(a)]. Our expectation for preferential coupling is borne out by comparison with the experiments, where we obtain a fairly good fit to the frequencies of the observed features for several void radii ($R = 1.9, 4.5, 6.5, 9.1$), but only to modes lying above the light line.

The agreement between theory and experiment is good despite the shortcomings of our model, most notably the fact that in reality the voids are far from spherical, having a significant aperture at the top [Fig. 3(c)]. Indeed, one of the features of the experimental data is that the strong modes shift very little in energy once half the sphere height has been reached (region II in Fig. 3). This suggests that the modes that are observed (which follow spherical harmonics $Y_{\ell m}$) are concentrated around the “equator” of the voids and so are perturbed relatively little by the top aperture. Such modes have the maximum azimuthal quantum number $|m| = \ell$, as shown in Fig. 4(c). The presence of the aperture will break the m degeneracy, leading to a more complicated mode structure, especially for the most distorted geometries where the eccentricity (defined by the ratio of maximum to minimum aperture radius) exceeds 1.5 [Fig. 3(c) and 3(d)]. This probably explains the extra modes which we observe experimentally, but a more realistic model is necessary to provide a full interpretation of their behavior. In particular, the progressive localization of surface plasmons in steadily deepening cups (region I) and the shielding of modes in nearly enclosed cavities (regions II to III) are of interest. The lack of dependence of the plasmon frequencies on the local geometry of nearest neighbors (which would otherwise smear out the resonances) confirms the localization of these states. Periodic arrays modify this picture only through interference phenomena leading to extra angular dependences. Further theoretical work is in progress to develop such a deeper model, including the external coupling to incoming light.

Localization of the plasmons in these metallic nanocavities is shown here by the dependence of the resonance energies on the void thickness, but not on the azimuthal or incident angles, together with the excellent agreement with our simple theory. Localized plasmons are analogous to electrons confined in quantum dots. The similar structure of Maxwell’s and Schrödinger’s equations provide similar solutions, but on different length scales, and suggest a range of possible applications for this technology. The negative curvature confinement increases the plasmon energies because a greater electric field overlap is produced in the surrounding air, increasing the electromagnetic energy densities. In contrast, the positive curvature metal surface reduces this energy density, resulting

in little confinement. A second significant difference between metal voids and metal spheres is the momentum required by photons to interact with the localized plasmons. Compared to the extremely small spheres that are difficult to tune in frequency, metallic voids with $1.33 < R < 10$ have plasmons in this well-defined cup geometry which strongly interact with impinging light, dominating diffraction effects. Thus tunable metallic optomolecular sensors and filters are a prospect. In addition, such nano-optical devices have unusual properties such as near-field collimators for chromophores arranged at the geometric center of the microcavities. Indeed we have recently shown that dropping a scanning-near-field optical tip into the spherical voids increases the retroreflected light by several orders of magnitude. In addition, we are also investigating magnetic photonic mesoporous metals. These materials are part of a general class of new “metamaterials” in which extra properties arise from selective nanoexcavation, which are not present in the ingredient components themselves. The ability to easily fabricate, at low cost, a large variety of such photonic metallic structures promises applicability in many diverse areas ranging from biotechnology to optoelectronics.

-
- [1] R. W. Wood, *Philos. Mag.* **4**, 396 (1902); *Phys. Rev.* **48**, 928 (1935).
 - [2] T. W. Ebbesen, H. J. Lezec, H. G. Ghaemi, T. Thio, and P. A. Wolff, *Nature (London)* **391**, 667 (1998).
 - [3] H. F. Ghaemi, T. Thio, D. E. Grupp, T. W. Ebbesen, and H. J. Lezec, *Phys. Rev. B* **58**, 6779 (1998).
 - [4] U. Kreibig and M. Vollmer, *Optical Properties of Metal Clusters* (Springer-Verlag, Berlin, 1995).
 - [5] R. D. Averitt, D. Sakar, and N. J. Halas, *Phys. Rev. Lett.* **78**, 4217 (1997).
 - [6] S. J. Oldenburg, J. B. Jackson, S. L. Wescott, and N. J. Halas, *Appl. Phys. Lett.* **75**, 2897 (1999).
 - [7] J. D. Joannopoulos, R. D. Meade, and J. N. Winn, *Photonic Crystals* (Princeton University Press, Princeton, 1995).
 - [8] W. L. Barnes, T. W. Preist, S. C. Kitson, and J. R. Sambles, *Phys. Rev. B* **54**, 6227 (1996).
 - [9] W. Y. Zhang *et al.*, *Phys. Rev. Lett.* **84**, 2853 (2000).
 - [10] P. N. Bartlett, P. R. Birkin, and M. A. Ghanem, *J. Chem. Soc. Chem. Commun.* **2000**, 1671 (2000); M. C. Netti *et al.*, *Adv. Mater.* **13**, 1368 (2001).
 - [11] M. C. Netti, M. B. D. Charlton, G. J. Parker, and J. J. Baumberg, *Appl. Phys. Lett.* **61**, 991 (2000).
 - [12] J. A. Porto and F. J. Garcia-Vidal, and J. B. Pendry, *Phys. Rev. Lett.* **83**, 2845 (1999).
 - [13] W.-C. Tan, T. W. Preist, J. R. Sambles, and N. P. Wanstall, *Phys. Rev. B* **59**, 12 661 (1999).
 - [14] H. Raether, *Surface Plasmons* (Springer-Verlag, Berlin, 1988).
 - [15] A. D. Boardman *Electromagnetic Surface Modes* (Wiley, Chichester, 1982).
 - [16] No surface plasmon solutions exist for the equivalent TE modes.